Physics Faculty Research & Creative Works

Physics

Using Geometry to Manipulate Long-Range Correlation of Light inside Disordered Media

Raktim Sarma

Alexey Yamilov
Missouri University of Science and Technology, yamilov@mst.edu

Pauf Neupane

Hui Cao

Recommended Citation

Using geometry to manipulate long-range correlation of light inside disordered media

Raktim Sarma,[1] Alexey Yamilov,[2,*] Pauf Neupane,[2] and Hui Cao[1,†]

[1]*Department of Applied Physics, Yale University, New Haven, Connecticut 06520, USA*
[2]*Department of Physics, Missouri University of Science and Technology, Rolla, Missouri 65409, USA*
(Received 10 May 2015; revised manuscript received 11 October 2015; published 5 November 2015)

We demonstrate an effective approach of modifying the long-range spatial correlation for light propagating inside random photonic waveguides by varying the shape of the waveguide. The functional form of spatial correlation is no longer universal in the regime of diffusive transport and becomes shape dependent due to the nonlocal nature of wave propagation. The spatial dependence of the correlation may become asymmetric for light incident from opposite ends of the waveguide. This work opens the door to control nonlocal effects in mesoscopic transport of waves by tailoring the geometry of random systems.

The diffusion model has been widely utilized to describe wave propagation in disordered media, e.g., light in biological tissues, ultrasonic waves through cracked metals, and electron wave functions in disordered conductors. It, however, ignores the interference of scattered waves, which lead to many prominent phenomena, including Anderson localization, universal conductance fluctuations, and enhanced backscattering [1–3]. Extensive theoretical and experimental studies in the past three decades have illustrated that mesoscopic transport of both classical and quantum mechanical waves is governed by wave interference effects [4,5].

One important consequence of wave interferences in random media is the correlations in the fluctuations of scattered intensities [6,7]. The interference between waves scattered along independent paths gives rise to an intensity correlation on the scale of a wavelength, where one crossing of paths generates long-range correlation beyond the mean free path, and two crossings lead to an infinite-range correlation [8,9].

The nonlocal correlations have direct consequences for the coherent control of light transmission through random media via wave-front shaping [10], which has advanced rapidly in the past few years due to potential applications to deep tissue imaging [11–13]. Indeed, focusing light on a single speckle simultaneously brightens nearby speckles, hence reducing the contrast of focusing [14,15]. It has been shown that the spatial correlation of intensity inside the random medium [16–20] determines not only focusing contrast but also energy deposition into the sample [21]. Moreover, the long-range correlation also affects the enhancement of total transmission [22] by an optimized wave front with a limited degree of input control [23]. Therefore, manipulating the nonlocal correlation can open up a new avenue to controlling waves inside random media.

Typically, the magnitude of long-range correlation is small, but it becomes significant in strongly scattering media, especially when the localization regime [3] is approached [8,9,24–27]. Experimentally long-range correlations have been observed not only in space, but also in time, frequency, angle, and polarization, but most measurements are performed on transmitted or reflected light, i.e., *outside* the random media

[17,19,28–34]. Modifications of the correlations of transmitted light have been realized with two techniques: (i) varying the spot size of an incident beam on a wide disordered slab [16,19,26], and (ii) inserting a constriction, e.g., a pinhole, inside a random medium [30,35]. However, the possibility of manipulating long-range correlations *inside* the random media has not been explored. This is at least in part due to the experimental challenge of gaining noninvasive access to the interior of a random structure where light propagates.

We recently fabricated quasi-two-dimensional random waveguides to probe the transport inside from the third dimension [20,36,37]. This experimental setup has enabled us to monitor directly how the long-range spatial correlations build up inside diffusive systems [20]. Moreover, by reducing (or increasing) the width of a rectangular waveguide, we were able to enhance (or suppress) the crossing probabilities of scattering paths throughout the system and, therefore, to modify the *magnitude* of the long-range correlation function. However, the functional form of correlation remained unchanged, as it is known to be universal for diffusive waveguides with uniform width [16,18].

In this Rapid Communication, we experimentally demonstrate an effective approach of tailoring the spatial dependence of long-range intensity correlation functions *inside* a random system. This is accomplished by fabricating photonic waveguides with the cross section varying along their length. The functional form of the long-range correlation is modified inside waveguides of different shapes because the crossing probability of scattering paths is affected nonuniformly in space. Our approach enables global optimization of nonlocal effects via system geometry and it is applicable to other types of waves, such as acoustic waves and matter waves. Besides the fundamental importance, manipulating the long-range correlation of waves inside random systems is useful for imaging and focusing into multiple scattering media using wave-front shaping [10,21,38] because it affects such aspects as focusing contrast, degree of control, as well as energy deposition inside the medium. Therefore, our approach can provide an additional degree of freedom for controlling wave transport in scattering media.

To illustrate the effects of waveguide geometry on long-range spatial correlation, we first present a theoretical analysis of two-dimensional (2D) disordered waveguides. The structures have reflecting sidewalls which confine the light

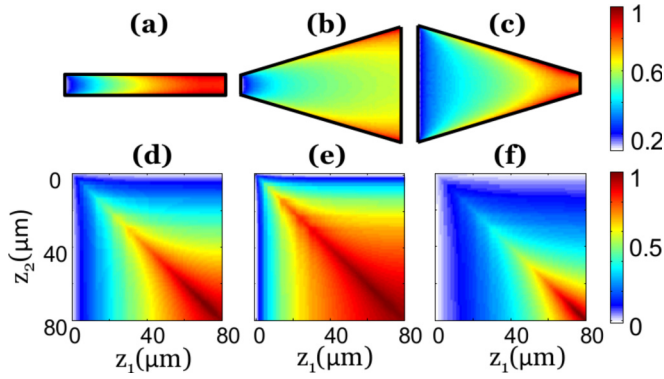————
*yamilov@mst.edu
†hui.cao@yale.edu

FIG. 1. (Color online) Calculated spatial long-range intensity correlation for the constant-width and two types of tapered 2D random waveguides. The waveguide length $L = 80\,\mu$m, the transport mean free path $\ell = 2.2\,\mu$m, and the diffusive absorption length $\xi_a = 26\,\mu$m. The waveguide in (a) and (d) has a constant width $W = 10\,\mu$m; in (b) and (e) $W(z)$ increases linearly from 10 to $60\,\mu$m, while in (c) and (f) $W(z)$ decreases linearly from 60 to $10\,\mu$m. (a)–(c) show the spatial distribution of the magnitude of the long-range correlation function $C_2(\mathbf{r};\mathbf{r})$ for three geometries. (d)–(f) show the long-range correlation function $C_2(z_1;z_2)$ of the cross-section averaged intensity [42] for the same geometries. The maximum value is normalized to 1 for comparison. The differences in these plots reveal that the waveguide geometry has a significant impact on the magnitude and range of C_2.

inside the waveguide where scattering and diffusion take place within the $\mathbf{r} = (y,z)$ plane, with z being the axial direction. Light transport in the random waveguide is diffusive, and the nonlocal intensity correlation is dominated by the long-range correlation C_2 [6,24]. The 2D correlation function $C_2(\mathbf{r}_1;\mathbf{r}_2)$ between two points $\mathbf{r}_1 = (y_1,z_1)$ and $\mathbf{r}_2 = (y_2,z_2)$ is calculated with the Langevin approach [18,19,39–41] (see Ref. [42] for details).

Let us consider the simplest case of linear tapering where the waveguide width [$W(z)$] increases or decreases linearly along the waveguide axis z. Figure 1 shows the magnitude of C_2, $C_2(\mathbf{r};\mathbf{r})$ in three waveguides, with $W(z)$ being constant [Fig. 1(a)], linear increasing [Fig. 1(b)], or linear decreasing [Fig. 1(c)]. The 2D distributions of C_2 across the waveguides are clearly different in the three cases, revealing that the waveguide geometry has a significant impact on the growth of C_2. In Figs. 1(d)–1(f), the correlation functions $C_2(z_1;z_2)$ of the cross-section averaged intensity [42] further illustrate the difference: In the waveguide of increasing $W(z)$, the correlation function stays nearly constant for most values of z_1 and z_2, while in the waveguide of decreasing width, the correlation function exhibits more rapid variation over z_1 and z_2. These results suggest that the range of spatial correlation is increased (or decreased) in the gradually expanding (or contracting) waveguide, as compared to the waveguide of constant width.

For a more quantitative comparison, the magnitude of C_2 of the cross-section averaged intensity, i.e., $C_2(z;z)$, is plotted in Fig. 2(a) for six waveguides of the same length but different geometry. To compare the shapes of these curves, the maximum value of each curve is set to 1. After the
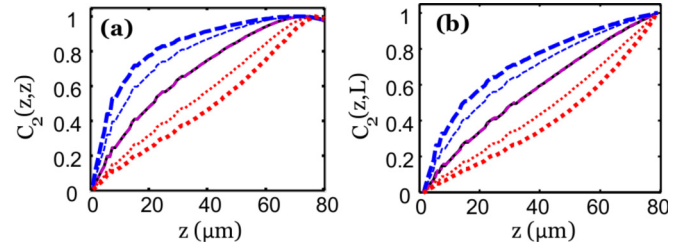

FIG. 2. (Color online) Comparison of calculated long-range correlation in six waveguides with different degrees of taper: two with constant widths of $10\,\mu$m (solid black line) and $60\,\mu$m (dashed-dotted magenta line); two with width linearly increasing from $10\,\mu$m (thick dashed blue line) or $20\,\mu$m (thin dashed blue line) to $60\,\mu$m; and two with width linearly decreasing from 60 to $10\,\mu$m (thick dotted red line) or $20\,\mu$m (thin dotted red line). Other parameters are the same as in Fig. 1. Both (a) $C_2(z;z)$ and (b) $C_2(z;L)$ clearly demonstrate that while the functional form of long-range correlation is universal for uniform waveguides, it is strongly modified in the tapered ones.

normalization, the two curves for the constant widths of 10 and $60\,\mu$m coincide and agree to the universal functional form. In the expanding waveguide, $C_2(z;z)$ increases more rapidly at the beginning and levels off when light diffuses deeper into the waveguide. This is attributed to the higher crossing probability of scattering paths near the front end of the waveguide where the cross section is narrower. As the width increases with z, the crossing probability is reduced, and the enhancement of C_2 is slowed down. The contracting waveguide exhibits the opposite trend: The magnitude of C_2 grows more quickly in the second half of the waveguide due to the enhanced crossing probability. We can further conclude that by enhancing the tapering of the waveguide cross section, the change in the spatial dependence of C_2 can be made larger.

Figure 2(b) plots the correlation function $C_2(z;L)$ for two points z and L of the cross-section averaged intensity of the six waveguides studied above. After normalizing the maximum value to 1, $C_2(z;L)$ for the two constant-width waveguides coincide; in the expanding waveguide the spatial range of correlation is enhanced while in the contracting waveguide the range is reduced. To be more quantitative, we find the correlation length Δz from $C_2(L - \Delta z; L) = C_2(L; L)/2$. The constant-width waveguides have the same $\Delta z = 48\,\mu$m, whereas the waveguide tapered from 10 to $60\,\mu$m has $\Delta z = 65\,\mu$m and the one from 60 to $10\,\mu$m has $\Delta z = 27\,\mu$m. Hence, the correlation length inside the random waveguide can be tuned by geometry.

We note that the change in the functional form of the long-range correlation function cannot be explained by the effective conductance model [42]. This model, which was developed in previous studies of expanding diffusive beams inside disordered slabs [26,30], can only predict the correlations of light outside random media. Inside a random medium, the magnitude of C_2 at depth z is not determined simply by the effective conductance of the waveguide section from 0 to z, which only reflects the crossing probability of scattering paths between 0 and z. The diffusive waves that pass through z may return to it after multiple scattering and crossing in the section between z and L, thus contributing to C_2 at z as well.

Indeed, the calculated C_2 inside the random waveguide of either constant or varying cross section displays a significant difference from the prediction of the effective conductance model [42].

Next, we conduct the experiments. The 2D disordered waveguides are fabricated in a silicon-on-insulator (SOI) wafer with a 220 nm silicon layer on top of a 3 μm buried oxide. The structures are patterned by electron beam lithography and etched in an inductively coupled plasma (ICP) reactive ion etcher (RIE). Each waveguide contains a 2D random array of air holes that scatter light. The air hole diameters are 100 nm and the average (center-to-center) distance of the adjacent holes is 390 nm. The waveguide walls are made of a triangle lattice of air holes (a lattice constant of 440 nm, and a hole radius of 154 nm) that has a complete 2D photonic band gap for the in-plane confinement of light.

The monochromatic beam from a tunable cw laser source (HP 8168F) is coupled into the empty waveguide by an objective lens of numerical aperture (NA) 0.4. The light is transverse-electric (TE) polarized, i.e., the electric field is in the plane of the waveguide. After propagating through the empty waveguide, the light is incident onto the random array of air holes inside the waveguide. The front end of the random array is uniformly illuminated along the y direction. The light undergoes multiple scattering in the 2D plane of waveguide. Some of the light is scattered out of plane and imaged by a 50$\times$ objective lens (NA = 0.42) onto an InGaAs camera (Xeva 1.7-320).

From the optical image, the spatial distribution of light intensity inside the waveguide $I(y,z)$ is extracted. To smooth out the short-range fluctuations, $I(y,z)$ is averaged over the cross section of the waveguide to obtain the cross-section averaged intensity $I_v(z)$. The spatial intensity correlation $C(z_1,z_2)$ is then computed from $I_v(z)$. With the short-range contribution removed, $C(z_1,z_2)$ is dominated by long-range correlation C_2. The contribution of C_3, which is on the order of $1/g^2$ (where g is the dimensionless conductance), is negligible as $g \gg 1$ in our waveguides.

The relevant parameters for light transport in the disordered waveguide are the transport mean free path l and the diffusive dissipation length ξ_a. The dissipation results from out-of-plane scattering, which can be treated similarly as absorption [36]. From the disordered waveguides with constant width, we find $\xi_a = 26$ μm and $\ell = 2.2$ μm by fitting the measured $I_v(z)$ and $C(z_1,z_2 = z_1)$ [42]. The tapered waveguides have the same density and diameter of the air holes, and thus the values of ξ_a and ℓ are identical.

Figures 3(a) and 3(b) are the scanning electron microscope (SEM) images of an expanding waveguide and a contracting waveguide. The measured correlation functions for the cross-section averaged intensity inside the two waveguides, $C(z_1 = z, z_2 = L)$, are plotted in Fig. 3(c). The experimental data clearly show that the dependence of $C(z,L)$ on z is very different for the two tapered waveguides, which agree well to the calculation results.

Since the waveguide geometry in Fig. 3(b) is the mirror image of the one in Fig. 3(a), the $C(z,L)$ for light input from the left end of the former is equivalent to that with input from the right end of the latter. As C is dominated by the long-range
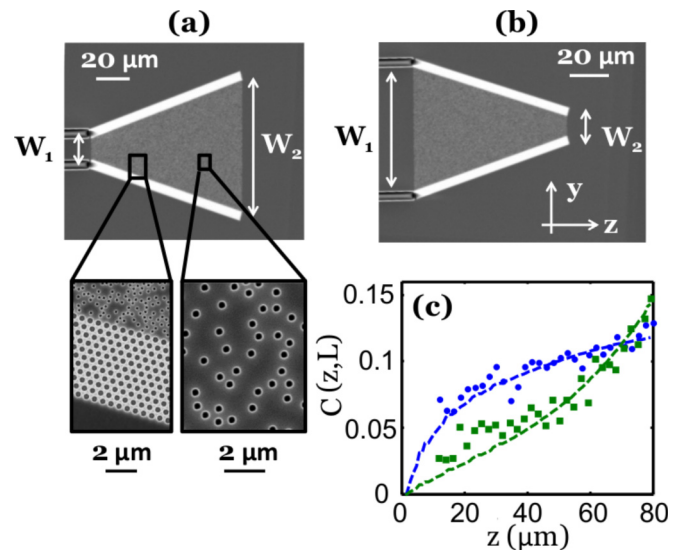

FIG. 3. (Color online) Experimental measurement of long-range intensity correlation inside the tapered waveguides. (a), (b) Top-view SEM images of fabricated quasi-2D disordered waveguides with linearly (a) increasing or (b) decreasing width. The width of the waveguide in (a) increases from 10 to 60 μm, and in (b) it is opposite. Both have the same length $L = 80$ μm. Magnified SEM images show the air holes distributed randomly in the tapered section of the waveguide and the triangle lattice of air holes in the reflecting sidewalls. (c) Measured long-range correlation function for the cross-section averaged intensity $C(z,L)$ inside the tapered waveguides shown in (a) and (b). The blue circles (green squares) represent experimental data for the waveguides with increasing (decreasing) width, and the dashed lines are theoretical results.

correlation function, this result implies C_2 becomes asymmetric. Note that the asymmetry exists only inside the random medium. The C_2 for the transmitted light remains symmetric, as it is determined by the dimensionless conductance g which has the same value for the two waveguides [42].

The difference in the correlation functions in expanding and contracting waveguides reveals that $C_2(\mathbf{r}_1; \mathbf{r}_2)$ is no longer symmetric because one waveguide is a mirror image of the other. In other words, the long-range intensity correlation function for light input from one end of the tapered waveguide is different from that with input from the other end. This behavior is distinct from that of the constant-width waveguide whose two ends are equivalent.

Next, we vary the waveguide cross section in a non-monotonic manner for further manipulation of the long-range intensity correlation inside the random waveguide. The waveguide shown in Fig. 4(a) has width W increasing linearly in the first half of the waveguide and decreasing in the second half. This geometry, unlike the tapered waveguides studied above, is symmetric with respect to the center ($z = L/2$), thus the spatial intensity correlation function is the same for light incident from either end of the waveguide. Figure 4(b) shows the spatial distribution of light intensity inside the waveguide with input from the left end. The short-range intensity fluctuations seen in Fig. 4(b) are smoothed out after the intensity is averaged over the cross section, leaving only the
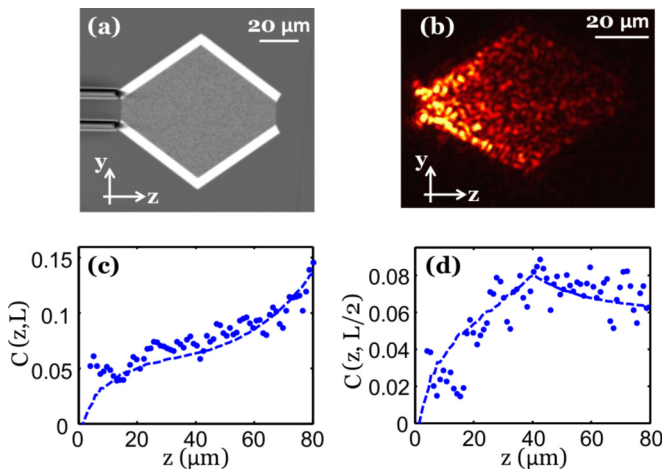
FIG. 4. (Color online) Long-range correlation in a quasi-2D disordered waveguide whose width varies nonmonotonically. (a) Top-view SEM image showing the waveguide width W increases linearly from 10 μm at $z = 0$ to 60 μm at $z = 40$ μm and then reduces linearly down to 10 μm at $z = 80$ μm. Other structural parameters are the same as the waveguides in Fig. 3. (b) An optical image of the intensity of scattered light from the disordered waveguide. The wavelength of the probe light is 1510 nm. (c) Long-range correlation function $C(z,L)$ for the cross-section averaged intensities at z and L in the waveguide shown in (a). $C(z,L)$ displays a sharp change in the growth rate before and after z passes $L/2$. (d) Long-range correlation function for the cross-section averaged intensities at z and $L/2$ in the waveguide shown in (a). $C(z,L/2)$ increases monotonically in the first half of the waveguide and decreases slightly in the second half. In (c) and (d), solid circles represent experimental data and the dashed curves are obtained by numerical calculation.

long-range contributions to the intensity correlation function $C(z_1,z_2)$. Figure 4(c) plots $C(z,L)$, which increases initially at a slow rate as z approaches $L/2$, but turns into a sharp rise once z passes $L/2$ and approaches L. This is because the crossing probability of scattering paths is first reduced as the waveguide is expanding in $z < L/2$, and then enhanced in $z > L/2$ as the cross section decreases. Therefore, the crossing probability can be controlled by modulating the waveguide width, which changes the spatial dependence of long-range correlation function. Figure 4(d) shows the intensity correlation function $C(z,L/2)$. It first increases monotonically as z moves from 0 to $L/2$, and then decreases slightly for z from $L/2$ to L. The experimental data (solid circles) are in good agreement to the theoretical results (dashed lines) in Figs. 4(c) and 4(d).

Finally, we comment that the confined geometry can be used to tailor the functional form of long-range correlations not only in real space, but also in momentum space [42]. The former sets the contrast for light focused inside a scattering medium by shaping the input wave front [15], whereas the latter determines the maximum total transmission that can be achieved with incomplete control of the input wave front [22]. Therefore, we believe our approach will have immediate applications to communication and imaging through or into turbid media [10].

[1] P. Sheng, *Introduction to Wave Scattering, Localization, and Mesoscopic Phenomena* (Academic, Boston, 1995).

[2] E. Akkermans and G. Montambaux, *Mesoscopic Physics of Electrons and Photons* (Cambridge University Press, Cambridge, UK, 2007).

[3] A. Lagendijk, B. van Tiggelen, and D. S. Wiersma, Phys. Today **62**(8), 24 (2009).

[4] B. L. Altshuler, P. A. Lee, and R. A. Webb, *Mesoscopic Phenomena in Solids* (North-Holland, Amsterdam, 1991).

[5] M. C. van Rossum and T. M. Nieuwenhuizen, Rev. Mod. Phys. **71**, 313 (1999).

[6] R. Berkovits and S. Feng, Phys. Rep. **238**, 135 (1994).

[7] R. Pnini, in *Correlation of Speckle in Random Media, Proceedings of the International Physics School on Waves and Imaging through Complex Media, 1999, Cargese, France*, edited by P. Sebbah (Kluwer Academic, Dordrecht, 2001), pp. 392–412.

[8] S. Feng, C. Kane, P. A. Lee, and A. D. Stone, Phys. Rev. Lett. **61**, 834 (1988).

[9] S. Feng and P. A. Lee, Science **251**, 633 (1991).

[10] A. P. Mosk, A. Lagendijk, G. Lerosey, and M. Fink, Nat. Photon. **6**, 283 (2012).

[11] Z. Yaqoob, D. Psaltis, M. S. Feld, and C. Yang, Nat. Photon. **2**, 110 (2008).

[12] X. Xu, H. Liu, and L. V. Wang, Nat. Photon. **5**, 154 (2011).

[13] H. Yu, J. Park, K. Lee, J. Yoon, K. Kim, S. Lee, and Y. K. Park, Curr. Appl. Phys. **15**, 632 (2015).

[14] I. M. Vellekoop and A. P. Mosk, Phys. Rev. Lett. **101**, 120601 (2008).

[15] M. Davy, Z. Shi, and A. Z. Genack, Phys. Rev. B **85**, 035105 (2012).

[16] R. Pnini and B. Shapiro, Phys. Rev. B **39**, 6986 (1989).

[17] A. Z. Genack, N. Garcia, and W. Polkosnik, Phys. Rev. Lett. **65**, 2129 (1990).

[18] A. A. Lisyansky and D. Livdan, Phys. Rev. B **47**, 14157 (1993).

[19] J. F. de Boer, M. P. van Albada, and A. Lagendijk, Phys. Rev. B **45**, 658 (1992).

[20] R. Sarma, A. Yamilov, P. Neupane, B. Shapiro, and H. Cao, Phys. Rev. B **90**, 014203 (2014).

[21] X. Cheng and A. Z. Genack, Opt. Lett. **39**, 6324 (2014).

[22] S. M. Popoff, A. Goetschy, S. F. Liew, A. D. Stone, and H. Cao, Phys. Rev. Lett. **112**, 133903 (2014).

[23] A. Goetschy and A. D. Stone, Phys. Rev. Lett. **111**, 063901 (2013).

[24] M. J. Stephen and G. Cwilich, Phys. Rev. Lett. **59**, 285 (1987).

[25] A. A. Chabanov, M. Stoytchev, and A. Z. Genack, Nature (London) **404**, 850 (2000).

[26] T. Strudley, T. Zehender, C. Blejean, E. Bakkers, and O. L. Muskens, Nat. Photon. **7**, 413 (2013).

[27] C. P. Lapointe, P. Zakharov, F. Enderli, T. Feurer, S. E. Skipetrov, and F. Scheffold, Europhys. Lett. **105**, 34002 (2014).

[28] M. P. van Albada, J. F. de Boer, and A. Lagendijk, Phys. Rev. Lett. **64**, 2787 (1990).

[29] N. Garcia, A. Z. Genack, R. Pnini, and B. Shapiro, Phys. Lett. A **176**, 458 (1993).

[30] F. Scheffold, W. Hartl, G. Maret, and E. Matijevic, Phys. Rev. B **56**, 10942 (1997).

[31] P. Sebbah, R. Pnini, and A. Z. Genack, Phys. Rev. E **62**, 7348 (2000).

[32] P. Sebbah, B. Hu, A. Z. Genack, R. Pnini, and B. Shapiro, Phys. Rev. Lett. **88**, 123901 (2002).

[33] A. A. Chabanov, N. P. Tregoures, B. A. van Tiggelen, and A. Z. Genack, Phys. Rev. Lett. **92**, 173901 (2004).

[34] O. L. Muskens, T. van der Beek, and A. Lagendijk, Phys. Rev. B **84**, 035106 (2011).

[35] F. Scheffold and G. Maret, Phys. Rev. Lett. **81**, 5800 (1998).

[36] A. G. Yamilov, R. Sarma, B. Redding, B. Payne, H. Noh, and H. Cao, Phys. Rev. Lett. **112**, 023904 (2014).

[37] R. Sarma, A. Yamilov, T. Golubev, and H. Cao, Appl. Phys. Lett. **105**, 041104 (2014).

[38] N. Fayard, A. Cazé, R. Pierrat, and R. Carminati, Phys. Rev. A **92**, 033827 (2015).

[39] B. Z. Spivak and A. Y. Zyuzin, in *Mesoscopic Phenomena in Solids*, edited by B. L. Altshuler, P. A. Lee, and R. A. Webb (Elsevier Science Publishers, Amsterdam, 1991), Chap. 2.

[40] R. Pnini and B. Shapiro, Phys. Lett. A **157**, 265 (1991).

[41] E. Kogan and M. Kaveh, Phys. Rev. B **45**, 1049 (1992).

[42] See Supplemental Material at http://link.aps.org/supplemental/10.1103/PhysRevB.92.180203 for additional simulation results.